7. Terui S, Terauchi T, Abe H, et al. On clinical usefulness of ^{201}Tl scintigraphy for the management of malignant soft-tissue tumors. *Ann Nucl Med* 1994;8:55–64.
8. Tamaki N, Kawamoto Y, Yonekura Y, et al. Regional metabolic abnormality in relation to perfusion and wall motion in patients with myocardial infarction: assessment with emission tomography using an iodinated branched fatty acid analog. *J Nucl Med* 1992;33:659–667.
9. Kurata C, Kobayashi A, Yamazaki N. Dual-tracer autoradiographic study with thallium-201 and radioiodinated fatty acid in cardiomyopathic hamsters. *J Nucl Med* 1989;30:80–87.
10. Scott WW Jr, Fishman EK. Soft-tissue masses. In: Scott WW Jr, Magid D, Fishman EK, eds. *Computed tomography of the musculoskeletal system.* New York: Churchill Livingstone;1987:1–27.
11. London J, Kim EE, Wallace S, Shirhoda A, Coan J, Evans H. MR imaging of liposarcomas: correlation of MR features and histology. *J Comput Assist Tomogr* 1989;13:832–835.
12. Sundaram M, Baran G, Merenda G, et al. Mixoid liposarcoma: magnetic resonance imaging appearance with clinical and histological correlation. *Skel Radiol* 1990;19:359–362.
13. Harms SE, Greenway G. Musculoskeletal system. In: Stark DD, Bradley WG Jr, eds. *Magnetic resonance imaging,* 2nd ed, vol. 2. St. Louis: Mosby; 1992:2107–2222.

Bone Metastasis with Superimposed Osteomyelitis in Prostate Cancer

Martha Pruckmayer, Christoph Glaser, Christian Nasel, Susanna Lang, Michael Rasse and Thomas Leitha
University Clinics of Nuclear Medicine, Maxillofacial Surgery, Radiology and Clinical Pathology, Vienna, Austria

The following case of a male patient with a history of prostate cancer suffering from pain and swelling in the right mandibular area illustrates the well-known diagnostic problem of a superinfected tumor. Orthopan tomography and CT showed no defects in bone structure or smooth tissue. Whole-body bone scanning showed increased tracer uptake in the mandibular bone and in several other locations in the skeletal system. Antigranulocyte immunoscintigraphy showed increased uptake over the right mandible, whereas the other metastatic sites were visualized as cold spots. A second CT scan depicted a sclerotic lesion with surrounding periostal reaction and soft-tissue swelling and was interpreted as osteomyelitis. Therefore, clinical symptoms, bone scanning, antigranulocyte immunoscintigraphy and follow-up CT resulted in a diagnosis of osteomyelitis, although open needle biopsy revealed the lesion to be prostate cancer metastasis with massive leukocytic invasion.

Key Words: antigranulocyte immunoscintigraphy; prostate cancer; bone metastases; SPECT

J Nucl Med 1996; 37:999–1001

Antigranulocyte immunoscintigraphy has been validated for the specific diagnosis and localization of focal granulocytic infections (*1–3*). The monoclonal antibody (MAb) 250/183 is a murine monoclonal Ig G1 antibody. It is directed against CEA nonspecific cross-reacting antigen (NC-95) exposed at the cellular membrane of peripheral granulocytes and myelocytes (*4*). About 80% of these are located in bone marrow (*5*). Two to 6 hr after administration, the labeled antibody normally accumulates in the liver, spleen and bone marrow (*6*). Its utility in detecting bone infection has been demonstrated (*1,2,7–11*).

In cancer patients, MAb 250/183 is utilized for bone marrow scanning. It indirectly visualizes the replacement of hematopoetic tissue in the bone marrow cavity by bone metastases as cold lesions (*12*). In contrast, bone scintigraphy visualizes osteoblastic metastases as hot spots due to the focal increase of osteoblastic activity. Thus, both diagnostic imaging procedures are used complementarily to image bone metastases (*13–15*), yet show similar tracer enhancement in osteomyelitis.

These concepts appeared feasible for application in the differential diagnosis of metastatic bone disease and osteomyelitis. In this report, we discuss the limitations of several imaging modalities in a case of metastatic tumor disease and superimposed osteomyelitis in the mandible.

Received Jul. 6, 1995; revision accepted Sept. 12, 1995.
For correspondence or reprints contact: Martha Pruckmayer, MD, University Clinic of Nuclear Medicine, General Hospital Vienna, Leitstelle 3L, Waehringer Guertel 18-20, A-1090 Vienna, Austria.

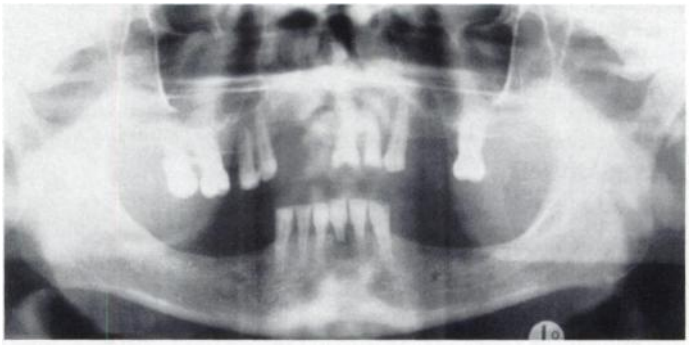

FIGURE 1. Orthopan tomography shows no sign of malignant destruction of the osseous structure in the right mandible.

CASE REPORT

A 62-yr-old man with a history of prostate cancer was examined because of progressive pain and swelling of the right mandibular region. Orthopan tomography showed no defects in bone structure in the mandibular region (Fig. 1). CT scans depicted no osteodestruction and thus appeared to be compatible with acute osteomyelitis.

Whole-body bone scintigraphy (3 hr postinjection of 600 MBq ^{99m}Tc-diphosphonate) indicated multiple sites of increased tracer uptake in several locations of the skeletal system, a phenomenon compatible with advanced metastatic disease (Fig. 2A). The local scintigram of the cranium showed increased tracer uptake over nearly the whole corpus of the right mandible. Because differential diagnosis between osteomyelitis and neoplastic lesions is not possible in static bone imaging alone, antigranulocyte immunoscintigraphy was recommended.

Bone scans and immunoscintigrams with MAb 250/183 were acquired with a double-headed gamma camera fitted with a low-energy, high-resolution, parallel-hole collimator (about 700,000 total counts). Antigranulocyte whole-body immunoscintigraphy was performed 6 hr after administration of 300 MBq radiolabeled BW 250/183. It showed typical cold lesions at the sites of hot spots on the bone scan, again consistent with the scintigraphic equivalent for metastatic marrow replacement (Fig. 2B). The mandibular hot spot on the bone scan was the only

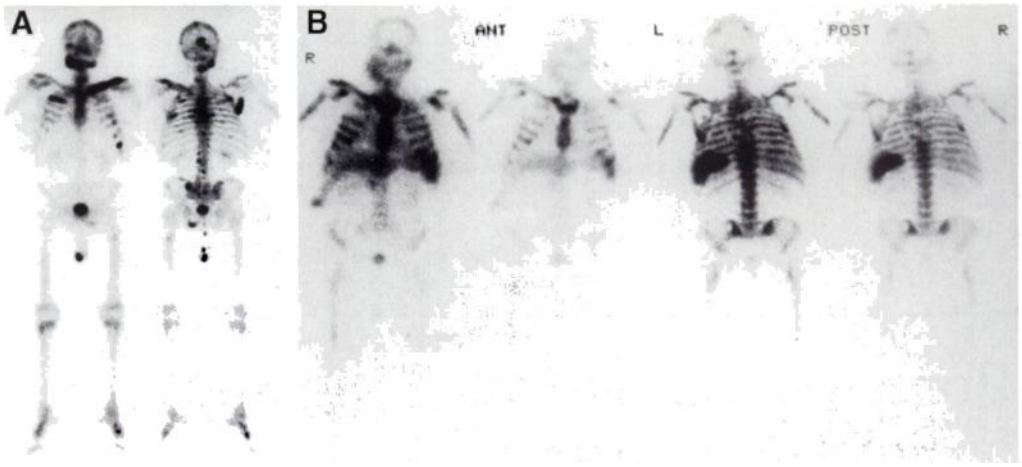

FIGURE 2. (A) Whole-body bone scan (anterior projection on the left, posterior projection on the right) shows multiple hot spots in the skeletal system, which are compatible with advanced metastatic disease. Note increased tracer uptake over the corpus of the right mandible. (B) Whole-body antigranulocyte immunoscintigraphy is given in two levels of intensity (anterior projection on the left, posterior projection on the right) to reveal bone marrow replacement in several locations matching the hot spots on the bone scan. Increased tracer uptake in the right mandibular bone is identical in shape and size to that on the bone scan.

exception. We found identically increased tracer uptake in the lesion in the right mandible.

SPECT images were acquired using a three-headed gamma camera with each head fitted with a low-energy, ultra high-resolution collimator (360°, 3°step, 40 sec/step). The raw data were processed using ramp filtered backprojection, three-dimensional postfiltering with a Wiener filter and reorientation in the transversal, coronal and sagittal slices. SPECT images revealed homogeneous tracer uptake in the whole lesion and failed to demonstrate a central cold lesion (Fig. 3).

A CT scan obtained after the SPECT study showed a small lucent focus with a sclerotic margin in the right mandible and soft-tissue swelling around this process (periosteal reaction) and was thought to be compatible with mandibular osteomyelitis. Thus, clinical symptoms, bone scans, antigranulocyte scans and follow-up CT all suggested the diagnosis of osteomyelitis. Consequently, the patient underwent antibiotic therapy and, initially, seemed to recover. However, a superinfected mandibular bone metastasis was a clinical possibility. Therefore, open needle biopsy was performed 2 wk after antigranulocyte immunoscintigraphy and revealed a metastasis of prostate cancer with massive leukocytic invasion.

DISCUSSION

This case illustrates the well-known diagnostic problem of a superinfected tumor. In this patient, all imaging techniques failed to reveal the underlying metastasis. Positive imaging of the mandibular metastasis in antigranulocyte immunoscintigraphy was obviously caused by the massive leukocytic infiltration of the tumor. Thus, in a strict sense, it cannot be accounted as a false-positive result. Granulocytes have been shown to accumulate within parenchymal tumors and malignant lesions (*16–18*). Another possible explanation for the "positive" antigranulocyte immunoscintigram could be that the antibody cross-reacts with CEA epitopes on tumor cells surfaces. CEA expression on prostate cancer cells is weak (*19–21*), but in advanced active cases, as in our patient, antigen shedding has been reported in up to 40% of the patients (*22*). We consider this uptake mechanism to be of minor importance in our patient because other metastatic lesions showed no antibody uptake.

Of note, the superimposed infection masks the photopenic defect, which should be found by bone marrow scintigraphy in metastatic lesions. Given the limited resolution of nuclear medical imaging, not even high-resolution SPECT was able to delineate the metastasis.

The distinct feature of this case is that the complementary utility of diphosphonate bone scanning and bone marrow scintigraphy will fail in patients with generalized metastatic disease and possible osteomyelitis. Additionally, none of the other imaging tools, orthopan tomography or CT found radiological proof for metastatic destruction. Moreover, a follow-up CT scan showed the typical picture of osteomyelitis. In this setting, invasive diagnosis seems mandatory to avoid the grave misdiagnosis of superinfected bone metastasis as osteomyelitis.

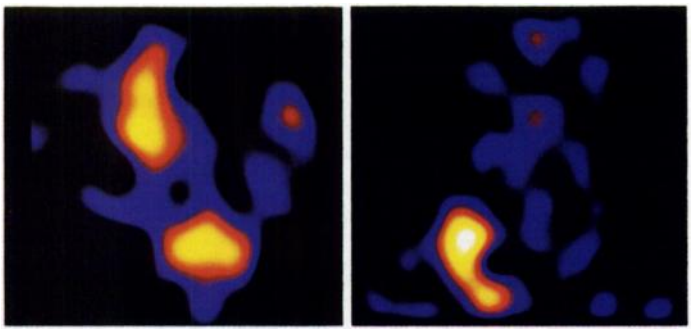

FIGURE 3. (A) Transaxial slice of high-resolution antigranulocyte SPECT (slice thickness 3.6 mm) through the mandible is on the left and (B) coronal slice is on the right. Both images show homogeneously increased tracer uptake in the corpus of the right mandibular bone and indicated no central cold spot that would be suspicious for a metastatic lesion.

REFERENCES

1. Locher JT, Seybold K, Andres RY, Schubinger PA, Mach JP, Buchegger F. Imaging of inflammatory and infectious lesions after injection of radioiodinated monoclonal antigranulocytes antibodies. *Nucl Med Commun* 1986;7:659–670.
2. Seybold K, Locher JT, Coosemans C, Andres RY, Schubinger A, Bläuenstein P. Immunoscintigraphic localization of inflammatory lesions: Clinical experience. *Eur J Nucl Med* 1988;13:587–593.
3. Farid NA, White SM, Heck LL. Technetium-99m-labeled leukocytes: preparation and use in identification of abscesses and tissue rejection. *Radiology* 1983;148:827–831.
4. Bosslet K, Lüben G, Schwarz A, et al. Immunohistochemical localization and molecular characteristics of three monoclonal antibody-defined epitopes detectable on carcinoembryonic antigen (CEA). *Int J Cancer* 1985;36:75–79.
5. Becker W, Borst U, Fischbach W, Pasurka B, Schäfer R, Börner W. Kinetic data of in vivo labeled granulocytes in humans with a murine ^{99m}Tc-labeled monoclonal antibody. *Eur J Nucl Med* 1989;15:361–366.
6. Joseph K, Höffken H, Damann V. In vivo labeling of granulocytes with ^{99m}Tc-labeled monoclonal antibodies: first clinical results. *Nuc Compact* 1987;18:223–229.
7. Becker W, Goldenberg DM, Wolf F. The use of monoclonal antibodies and antibody fragments in the imaging of infectious lesions. *Semin Nucl Med* 1994;24:142–153.
8. Dominquez Gadea L, Martin Curto LM, de la Calle H, Crespo A. Diabetic foot infections: scintigraphic evaluation with ^{99m}Tc-labeled antigranulocyte antibodies. *Nucl Med Commun* 1993;14:212–218.
9. Lind P, Langsteger W, Koltringer P, Dimai HP, Passl R, Eber O. Immunoscintigraphy of inflammatory processes with a technetium-99m-labeled monoclonal antigranulocyte antibody (MAb BW 250/183). *J Nucl Med* 1990;31:417–423.
10. Seybold K, Frey LD, Locher J. Immunoscintigraphy of infections using ^{123}I and ^{99m}Tc-labeled monoclonal antibodies. Advanced experiences in 230 patients. *Angiology* 1992;43:85–90.
11. Peltier P, Potel G, Lovat E, Baron D, Chatal JF. Detection of lung and bone infection with antigranulocyte monoclonal antibody BW 250/183 radiolabeled with ^{99m}Tc. *Nucl Med Commun* 1993;14:766–774.
12. Munz DL, Kornemann R, Brandhorst I, Hör G. Bone marrow scanning versus bone scanning in the early diagnosis of neoplastic involvement of the skeletal system. In:

Schmidt HAE, Adam WE. *Nuclear medicine: imaging of metabolisms and organ functions.* Stuttgart: Schattauer; 1984:644.
13. Bathmann J, Moser E. Comparison of skeletal scintigraphy and bone marrow scintigraphy in detection of osseous metastases. *Radiology* 1995;35:8–14.
14. Reske S, Kartsens J, Sohn M, Glockner W, Buell U. Bone marrow immunoscintigraphy compared with conventional bone scintigraphy for the detection of bone metastases. *Acta Oncol* 1993;32:753–761.
15. Otsuka N, Fukunaga M, Sone T, et al. The usefulness of bone marrow scintigraphy in the detection of bone metastasis from prostatic cancer. *Eur J Nucl Med* 1985;11:319–322.
16. Sfakianakis GN, Mnaymneh W, Ghandur-Mnaymneh L, Al-Sheikh W, Hourani M, Heal A. Positive indium-111-leukocyte scintigraphy in a skeletal metastasis. *Am J Radiol* 1982;139:601–603.
17. Leitha T, Stümpflen A, Gebauer A, Amann G, Dudczak R. "False positive" immunoscintigraphic diagnosis of liver abscesses in a patient with a necrotic liver tumor. *Eur J Nucl Med* 1989;15:673–675.
18. Fawcett HD, Lantieri RL, Frankel A, McDougall IR. Differentiating hepatic abscess from tumor: combined ^{111}In-white blood cell and ^{99m}Tc liver scans. *Am J Radiol* 1980;135:53–56.
19. Purnell DM, Heatfield BM, Trump BF. Immunocytochemical evaluation of human prostatic carcinomas for carcinoembryonic antigen, nonspecific cross-reacting antigen, beta-chorionic gonadotrophin and prostate-specific antigen. *Cancer Res* 1984;44:285–292.
20. Frkovic-Grazio S, Kraljic I, Trnski D, Tarle M. Immunohistochemical staining and serotest markers during development of a sarcomatoid and small cell prostate tumor. *Anticancer Res* 1994;14:2151–2156.
21. Tarle M. Serial measurements of tissue plypeptide-specific antigen, PSA, PAP and CEA serotest values in treated patients with primary and metastatic prostate cancer. *Anticancer Res* 1993;13:769–777.
22. Friedman RB, Anderson RE, Entine SM, Shelley BH. Effects of disease on clinical laboratory tests. *Clin Chem* 1980;26:280D.

Technetium-99m-Sestamibi Uptake in Myeloma

Bruce K. Adams, Abdulbasier Fataar and Mohammad A. Nizami
Department of Nuclear Medicine, University of Cape Town and Groote Schuur Hospital, Cape Town, South Africa

A number of reports describe how ^{99m}Tc-sestamibi detects benign and malignant primary and metastatic tumors. We report abnormal ^{99m}Tc-sestamibi uptake in nine sites in a 53-yr-old patient with histologically and biochemically proven IgG kappa-secreting myeloma. The ^{99m}Tc-sestamibi study was undertaken for an unrelated hyperparathyroidism.

Key Words: technetium-99m-sestamibi; myeloma

J Nucl Med 1996; 37:1001–1002

Although ^{99m}Tc-sestamibi was originally developed as a myocardial imaging agent it has been found to have many other useful applications. It has been used to detect benign tumors as well as several primary malignancies and metastatic tumors including: brain tumors (*1,2*), benign and malignant thyroid (*3–5*) and parathyroid tumors (*6,7*), breast carcinoma (*8*), lung carcinomas (*9,10*), non-Hodgkin's lymphoma (*11*), Burkitt's lymphoma (*12*), renal cell carcinoma (*12*), nasopharangeal carcinoma (*13*), carcinoid tumor (*14*), pancreatic Vipoma (*15*), ectopic ACTH-producing tumor (*16*), acoustic schwannoma (*17*), malignant thymoma (*12*) and osteosarcoma (*18*).

Moreover, ^{201}Tl-chloride uptake in the bone marrow of a patient with nonsecretory myeloma has been described (*19*). We report a case of ^{99m}Tc-sestamibi uptake in myeloma.

CASE REPORT

A 53-yr-old woman presented with a 1-mo history of mild confusion, abdominal cramps, vomiting and constipation. Physical examination revealed an ill lady with pallor and dehydration. She was confused with a depressed level of consciousness. Radiological examination revealed lytic lesions in the left frontal region of the skull, the upper thoracic vertebrae and the lateral aspect of the left clavicle.

The laboratory findings were: total serum calcium 3.31 mmol/liter (normal 2.1–2.6), ionized calcium 1.46 mmol/liter (normal 1.1–1.2), alkaline phospatase 201 U/liter (normal 30–70), parathormone 120 pg/ml (normal 10–55), inorganic phosphate 1.2 mmol/liter (normal 0.8–1.4), serum urea 19.9 mmol/liter (normal 1.7–6.7) and creatinine 217 mmol/liter (normal 75–115). The hemoglobin was 9.9 g/dl.

Other investigations including chest radiographs, mammography, intravenous pyelography, renal ultrasound, gastroscopy and sigmoidoscopy were all reported as normal. Ultrasound of the neck showed a lesion in the inferior pole of the left thyroid lobe.

Technetium-99m-sestamibi scintigraphy was performed in an attempt to detect possible parathyroid pathology. The patient received an intravenous injection of 500 MBq ^{99m}Tc-sestamibi. Anterior images of the neck were taken 15 min and 2 hr after injection using a gamma camera fitted with a low-energy, high-resolution collimator. Because the images showed multiple abnormal foci in the chest additional anterior images of the chest and skull were taken for 200 sec. The patient's condition deteriorated during the scanning procedure and she was returned to the intensive care unit before views of the spine could be obtained.

The ^{99m}Tc-sestamibi scan (Fig. 1) demonstrated diffusely increased uptake in the region of the inferior pole of the left thyroid lobe at 15 min postinjection, which was still visible at 2 hr. Figure 2 shows a number of abnormal foci in the anterior ribs, the lateral aspect of the left shoulder and clavicle and left frontal region of the skull. The latter two lesions corresponded to lytic areas on the radiographs, and the skull focus to a large frontal defect on CT. The neck was explored surgically. Parathyroid hyperplasia was discovered and three of the glands were removed.

A needle biopsy was taken of the skull lesion and histological examination was positive for myeloma. Urine examination revealed Bence-Jones protein with excessive amounts of IgG kappa light chains. A diagnosis of IgG kappa-secreting myeloma was made. The patient developed a polyneuropathy and her renal function deteriorated rapidly. Her condition continued to deteriorate despite assisted respiration and dialysis. She died as a result of her illness 2 mo later.

DISCUSSION

Although ^{99m}Tc-sestamibi is used chiefly for myocardial imaging, like its counterpart, ^{201}Tl-chloride, it is gaining recognition as a tumor imaging agent. The mechanism by which it concentrates in malignant tissue is not clear. Technetium-99m-sestamibi is sequestered in the cytoplasm and mitochon-

Received Jul. 10, 1995; revision accepted Oct. 25, 1995.
For correspondence contact: B.K. Adams, MD, Department of Nuclear Medicine, Groote Schuur Hospital, Observatory 7925, Cape Town, South Africa.